EurJOC
European Journal of Organic Chemistry

Research Article
doi.org/10.1002/ejoc.202500557

Chemistry Europe
European Chemical Societies Publishing

www.eurjoc.org

A Fullerene-Based Selenosugar Ball

Reinier Lemos,* Yoana Pérez-Badell, Mauro De Nisco, Giovanna Cimmino, Claudia González, Andrea Carpentieri, Severina Pacifico, Margarita Suárez,* and Silvana Pedatella*

Fullerenes functionalized with selenosugar moieties are of particular interest because of their important properties, as one fragment enhances the properties of the other. Selenosugars are not only solubilizing groups, but their intrinsic biological properties also provide additional attractive features to the conjugates. Here the synthesis is reported of a fullerene hexakis-adduct decorated with 12 peripheral seleno-D-talitol moieties with a T_h-symmetric structure, which can be efficiently synthesized from the hexakis-adduct of [60]fullerene prepared via a cycloaddition reaction and subsequent copper-catalyzed azide-alkyne cycloaddition click chemistry. This large-scale system, refer to as the selenosugar ball (SeB), has been characterized by ^{1}H NMR and ^{13}C NMR spectroscopy, mass spectrometry, UV-spectroscopy, and dynamic light scattering (DLS). Theoretical calculations using the multilevel DFT-B3LYP-D3(BJ)/6–311 G(2 d,p)//PM7 methodology are performed to predict the most stable conformation for the compound and to determine the factors that control the geometry of this molecule. In addition, some physicochemical parameters are estimated. Also, this new compound is tested on human keratinocyte HaCaT cells to determine its cytotoxicity and potential applications.

1. Introduction

Reactive oxygen species (ROS) represent a group of molecules that undergo continuous formation, transformation, and elimination in living organisms. The excessive formation of these species without efficient consumption generates the greatest oxidative stress and the deterioration of tissues and organs.[1] Antioxidants have received attention due to their ability to destroy free radicals, ROS, and reactive nitrogen species. Among the most studied antioxidants are vitamins such as ascorbic acid,[2] carotenes,[3] and even seleno-containing compounds.[4]

The seleno-containing compounds receive special interest due to the possibility of inserting this chalcogen-type atom into molecules with antioxidant power to enhance their effect and generate new ones. Selenium has been used to boost the effects of natural products such as polyphenols, amino acids, and carbohydrates.[5] A synergistic effect has been observed between selenium and the organic molecule, especially for sugars.[6]

Traditionally, antioxidants have been supplied orally, but the body assimilates only a small amount. One of the main causes is that antioxidants are destroyed by the presence of enzymes and the stomach's acidic environment.[7] Among the strategies studied for administering antioxidants are their encapsulation or conjugation to biological transporters.[8] Likewise, systems with nanometric dimensions that are also stable in the blood manage to cross the blood-brain barrier and transport drugs to the brain.[9] Recent studies demonstrate the use of nano-antioxidants to combat oxidative stress in the brain, allowing the detection of amyloid plaques,[10] and having anticonvulsant properties.[11]

Carbon nanoforms, such as nanotubes and fullerenes, are promising molecules for developing nano-antioxidants. In addition to the capacity to generate nanoparticles through their aggregation, fullerenes can effectively neutralize ROS by their addition to the double bonds.[12] There are several examples of hybrid fullerenes with potential antioxidant applications. Water-soluble potassium fullerenolates cause a decrease in cellular ROS in human embryonic lung fibroblasts over a wide range of concentrations.[13] Also, sugar-pendant [60]fullerenes containing glucose oligomers inhibited the free radical-induced lipid peroxidation in human plasma concentration-dependent doses analogous to antioxidant

R. Lemos, M. Suárez
Laboratorio de Síntesis Orgánica
Facultad de Química
Universidad de la Habana
10400 La Habana, Cuba
E-mail: reinier.lemos@fq.uh.cu
msuarez@fq.uh.cu

R. Lemos, C. González, A. Carpentieri, S. Pedatella
Department of Chemical Sciences
University of Napoli Federico II
Via Cintia 4, I-80126 Napoli, Italy
E-mail: pedatell@unina.it

Y. Pérez-Badell
Laboratorio de Química Computacional y Teórica
Facultad de Química
Universidad de la Habana
10400 La Habana, Cuba

M. De Nisco
Department of Health Sciences
University of Basilicata
Viale dell'Ateneo Lucano 10, I-85100 Potenza, Italy

G. Cimmino, S. Pacifico
Department of Environmental
Biological, and Pharmaceutical Sciences and Technologies
University of Campania "Luigi Vanvitelli"
Via Vivaldi 43, 81100 Caserta, Italy

Supporting information for this article is available on the WWW under https://doi.org/10.1002/ejoc.202500557

Research Article
doi.org/10.1002/ejoc.202500557

polyphenols.[14] We have recently reported on the functionalization of [60]fullerene with selenosugars and steroids as potential inhibitors of the aggregation of the β-amyloid peptide.[15] Moreover, an in vitro study of the ROS scavenging capacity of mono and poly methano[60]fullerenes showed good radical elimination in all cases. It was determined that hexa-substitution was the most promising for developing antioxidants.[16]

One of the most studied methods to functionalize fullerenes is the Bingel–Hirsch protocol.[17] In this reaction, a bifunctional malonic derivative is introduced on the fullerene's surface and serves as a valuable starting material for further side-chain modification. Depending on the reaction time, mono- or polyadducts can be isolated.[18]

C_{60} hexakis-adducts with T_h-symmetric addition patterns can be obtained by nucleophilic cycloadditions and cyclopropanations,[19] including various templating and anchoring techniques. C_{60} is a central building block for elaborating an esthetically pleasing and unique structural motif in organic chemistry.[20] These symmetric 3D macromolecular structures represent a class of stable polyadducts that are easy to prepare and have been studied for their application in various fields. Highlights include fullerene modified with biomolecules or bioactive fragments such as pendant DNA fragments,[21] peptides,[22] and pyridine derivatives.[23] Although obtaining hexakis-adduct derivatives is reported, most research has focused on incorporating sugars into these systems.[24] Due to the ability of carbohydrates to interact with lectins on the surface of cells and participate in cell growth and differentiation, the "Sugar Balls" have produced compounds with biological properties.[25] Systems containing fucose and mannose allow recognition through cell membrane lectins, and the potential applications of glycofullerenes in medicinal chemistry.[26] Considering the presence of dendritic cell-specific intercellular adhesion molecule-3-grabbing nonintegrin (DC-SIGN) on the surface of pathogens such as HIV and Ebola, these hybrids present promising antiviral properties. Martin and coworkers prepared globular glycofullerenes combining trimannosylated glycodendrons with a Bingel–Hirsch hexakis-adduct of [60]fullerene with 36 mannoses, and in the study of the biological activity of these glycomimetic hybrids in a cellular infection model, they were pioneers.[27] Later, the same research group developed novel multivalence tridecafullerenes appended with up to 360 units of 1,2-mannobiosides that showed outstanding activity in the picomolar range against zika and dengue infections.[28]

Sugar balls have also been decorated with iminosugar.[29] Incorporating glucose or mannose-containing nitrogen atoms was used to develop new ligands for lectins and glycosidases.[30] The multivalency of these systems is attributed to the structure and availability of the iminosugars of carbohydrate-binding areas.

The properties found for glycofullerenes show the successful combination of fullerenes with monosaccharides in generating multipurpose systems.[31] Therefore, considering the biological properties of selenium-containing compounds, incorporating selenium into a monosaccharide is a strategy to deliver it camouflaged in a biomolecule. In this way, selenosugars could be recognized by carbohydrate receptors and facilitate selenium action.

Therefore, in the framework of our research focused on the search for fullerene-based hybrids, in this work, we have designed and synthesized a C_{60} hexakis-adduct with a T_h-symmetric octahedral addition pattern decorated with selenosugar fragments named selenosugar balls (SeB). The Bingel cyclopropanation and the click chemistry methodologies were used to obtain the SeB, which was fully characterized by mass-spectrometric, NMR spectroscopic (1D and 2D), UV spectroscopic, and dynamic light scattering (DLS) analyses. To understand the influence of the interactions between the appendants in the molecule, density functional theory (DFT) calculations were performed to determine the most stable conformation and predict its electronic parameters. In order to obtain a preliminary criterion of cytotoxicity, SeB was tested in human keratinocyte HaCaT cells.

2. Results and Discussion

The synthetic route to obtain the symmetric SeB endowed with 12 selenium-containing D-talose units was carried out by a multistep synthetic procedure using click chemistry,[30] see **Scheme 1**.

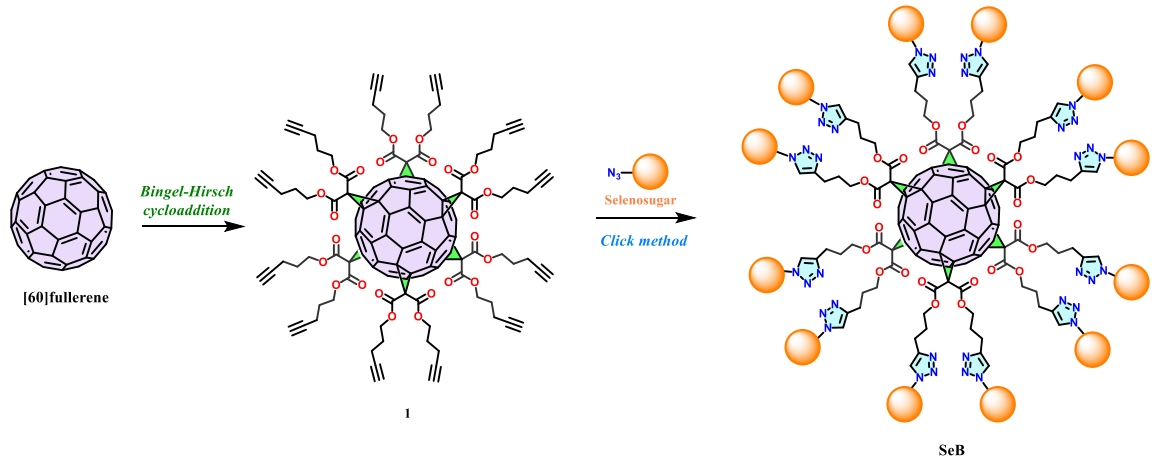

Scheme 1. General synthetic strategy for SeB.

Research Article
doi.org/10.1002/ejoc.202500557

Chemistry Europe
European Chemical Societies Publishing

Initially, precursor **1** was obtained through two synthetic steps, as shown in **Scheme 2**. By traditional esterification conditions, commercially available malonyl dichloride (**2**) was transformed into a di(pent-4-yn-1-yl) malonate (**3**).[32] This transformation employed dichloromethane as a solvent and basic conditions to neutralize the hydrochloric acid generated. Malonate **3** was obtained in 70% yield after purification by column chromatography using chloroform as eluent. Then, the [60]fullerene core was functionalized with six units of **3** by a cyclopropanation reaction under Bingel–Hirsch conditions, following the methodology previously reported.[30] In this reaction, the malonate derivative was added to C_{60} in toluene, employing 1,8-Diazabicyclo[5.4.0]undec-7-ene (DBU) and an excess of CBr_4.[29] The reaction occurs through several stages, depending on the number of incorporated moieties. In the first two hours, the reaction mixture color changes from purple to brown, due to the formation of the fullerene monoadduct. After 72 h, a red solution is formed, corresponding to polyadducts of [60]fullerene. Finally, the crude was purified by column chromatography, and compound **1** was isolated in 60% yield, which is similar to those reported for other hexakis[60]fullerenes.[33]

The reactivity of the terminal alkynes is used to efficiently and easily bind the seleno-containing compound by the azide-alkyne cycloaddition to the malonic linker. To continue the study of selenosugar-fullerene hybrids recently introduced by our research group,[15] we proposed extending the use of 4-seleno-D-ribose and included the 1,4-anhydro-4-seleno-D-talitol (SeTal) in the synthesis of hexakis[60]fullerenes. Considering the validated antioxidant in vitro and wound-healing properties of glyconjugates containing 4-seleno-D-ribose,[6a,8b] and the well-known antioxidant properties reported for SeTal,[6b] both selenosugars represent attractive moieties to incorporate into fullerene. The initial attempt focused on obtaining an azide derivative through the functionalization of **6** by introducing a suitable leaving group, yielding compound **7**, see **Scheme 3**. The functionalization of **6** was tested with different leaving groups such as iodine, mesyl, and tosyl, and in no case were the desired products detected. A mixture of products of difficult separation and identification was obtained. This behavior is related to the presence of a selenium atom in this ring since it can carry out an intramolecular nucleophilic substitution and replace the leaving group. Previous work with five-membered selenosugars has shown that the selenium atom can substitute good leaving groups in the C5 position on 4-selenium-D-ribose, generating a mix of unexpected products.[34]

SeTal in its furanose forms presents a side-chain with two hydroxyl groups, which can be functionalized with a leaving group. SeTal has an additional hydroxyl group absent in **6** that provides greater polarity to the final hybrid and could increase interaction with biological receptors. Under basic conditions, mono isopropylidene SeTal (**8**) was successfully transformed into a tosyl derivative **9** with a 77% yield. The secondary hydroxyl group remains untransformed, allowing tosylation without selenium interference. Compound **9** and sodium azide were dissolved in anhydrous *N*,*N*-dimethylformamide (DMF) at 100 °C overnight to obtain **10** in 70% yield.

^{1}H-NMR spectroscopy allows us to verify the formation of tosylate **9** and its transformation into the azide **10**. The signals of the aromatic protons in the tosyl group (7.78–7.35 ppm) disappear with the formation of **10**. In compound **9**, the signals of the protons attached to C6 are observed at ≈4.00 ppm, both as a doublet of the doublet, while this signal in **10** is deshielded and appears as a multiplet at 3.39–3.32 ppm. For both compounds, the rest of the

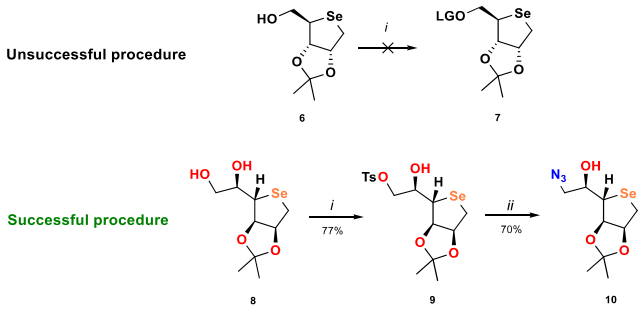

Scheme 3. Azide functionalization of selenoderivatives **6** and **8**. Conditions: *i*: *p*-toluenesulfonyl chloride (TsCl), triethylamine, DMAP, anhydrous DCM, r.t., o.n., *ii*: sodium azide, anhydrous DMF, 100 °C, o.n.

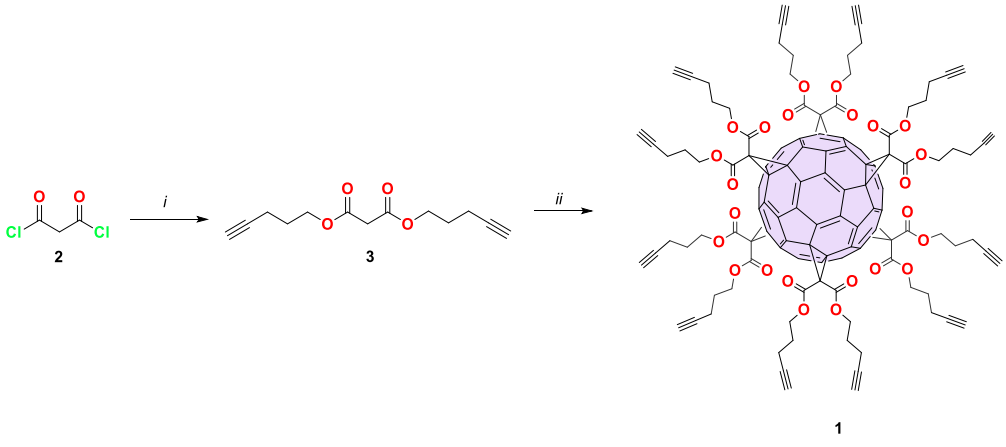

Scheme 2. Synthesis of the hexakis-adduct **1**. Conditions: *i*. pent-4-yn-1-ol, triethylamine, 4-dimethylaminopyridine (DMAP), dicloromethane (DCM), 0 °C to r.t., 4 h, 70%; *ii*. C_{60}, CBr_4, DBU, anhydrous toluene, 72 h, 60%.

Research Article
doi.org/10.1002/ejoc.202500557

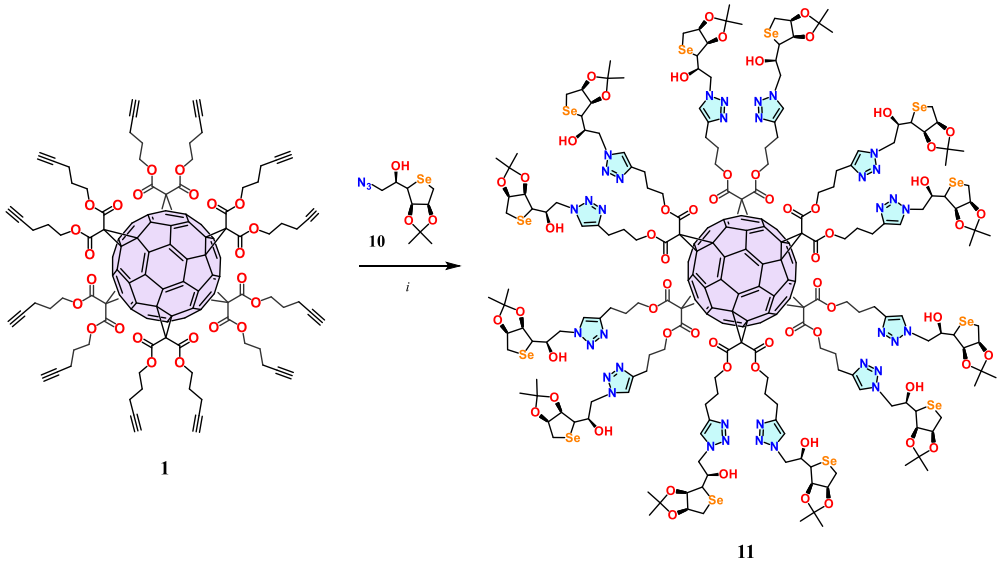

Scheme 4. Synthesis of **11**. Conditions: *i*: ascorbic acid, $CuSO_4{\cdot}5H_2O$, DCM/H_2O, r.t., 72 h, 80%.

signals are quite similar in position and multiplicity, see Figure S1–S10, Supporting Information.

The azide derivative **10** is efficiently incorporated into fullerene appendants by a triazole ring, as is represented in **Scheme 4**. The click coupling takes place by the copper-mediated Huisgen 1,3-dipolar cycloaddition of azides and alkynes in a dichloromethane-water mixture. Catalytic conditions promoted by Cu(I) generated in situ by reducing Cu(II) in the presence of sodium ascorbate are used. After 72 h, a satisfactory functionalization of all the fullerenes is achieved, and after a chromatographic separation, **11** is isolated with 80% yield as orange crystals.

An exhaustive characterization was carried out to corroborate the transformations in the different stages of the fullerene's modification using spectroscopic and analytical techniques. The octahedral substitution pattern was confirmed by analyzing the ^{13}C-NMR. Unlike lower adducts, where many C_{60} signals are observed, for hexakis-adducts, only two signals corresponding to the [60]fullerene skeleton are identified due to their T_h-symmetrical structure. This observation determines the highest degree of substitution without the presence of lower derivatives. Specifically, for **11** the sp^2 carbon signals of fullerene are found at 145.9 and 141.3 ppm, see **Figure 1**.

Mass spectrometry was employed to confirm the proposed structure of fullerene polyadducts. Figures S18, S17, Supporting Information show the mass spectra of **11** and precursor **1**, respectively. The HRMS-MALDI spectrum of **11** shows a peak at 4751.8940, which corresponds to a mass loss of 888 u from the molecular ion. This value corresponds to the mass of the isopropylidene groups of the 12 selenosugar moieties. Since the NMR characterization of **11** clearly shows its structure as is, this result is due to fragmentation phenomena during the recording of the spectrum. This behavior is analogous to our group's previous work with selenosugars conjugated to fullerenes.[15] Figure S19, Supporting Information shows the UV–vis spectra of **11** recorded in chloroform at two concentrations. In the spectra, the typical bands of the reported hexakis[60]fullerene are identified and grouped into two main regions.[30] The first, of lesser intensity, corresponds to the maxima at $\lambda = 317$ and 337 nm, and the second one, more intense at $\lambda = 269$ and 281 nm.

Considering the solubility of **11**, it can be commented that it produces highly colored orange solutions in common solvents such as chloroform, dichloromethane, dimethylformamide, and dimethyl sulfoxide (DMSO). Furthermore, it can dissolve efficiently in mixtures of water with DMSO. For a better understanding of the aggregation properties of SeB, the hydrodynamic distribution profiles in water were analyzed by DLS. **Figure 2** shows the size distribution found, where the particles were composed mainly of three populations: A (≈7 nm), B (≈100 nm), and C (≈1000 nm), depending on the solvent system used. In water, two populations, B and C, are identified, showing a high tendency to aggregation and a lower distribution centered on 1000 nm, with a polydispersity index (PDI) of 0.32. In a mixture of H_2O:DMSO (9:1), it is observed that the B population increases and the PDI (0.27) slightly decreases. Finally, the lowest degree of aggregation was found for H_2O:DMSO (8:2) mixture, where it was possible to identify a single population of ≈7 nm corresponding to two molecules of **11** aggregated. In this case, the PDI (0.16) reaches the minimum value among the systems studied and falls within the recommended range for the use of nanocarriers.[9b] The observed aggregation behavior corresponds with other biologically active glycofullerenes studied, which suggests its potential use in biological assays in water solutions.[22,27]

As part of the basic research aimed at understanding the geometric and electronic properties of the novel structure of **11** to estimate its future applications, theoretical calculations were carried out. Theoretical multilevel calculations (DFT-B3LYP-D3(BJ)/6–311 G(2 d,p)//PM7) have been performed to shed light on conformation and electronic properties. **Figure 3**A shows the

Research Article
doi.org/10.1002/ejoc.202500557

Chemistry Europe
European Chemical Societies Publishing

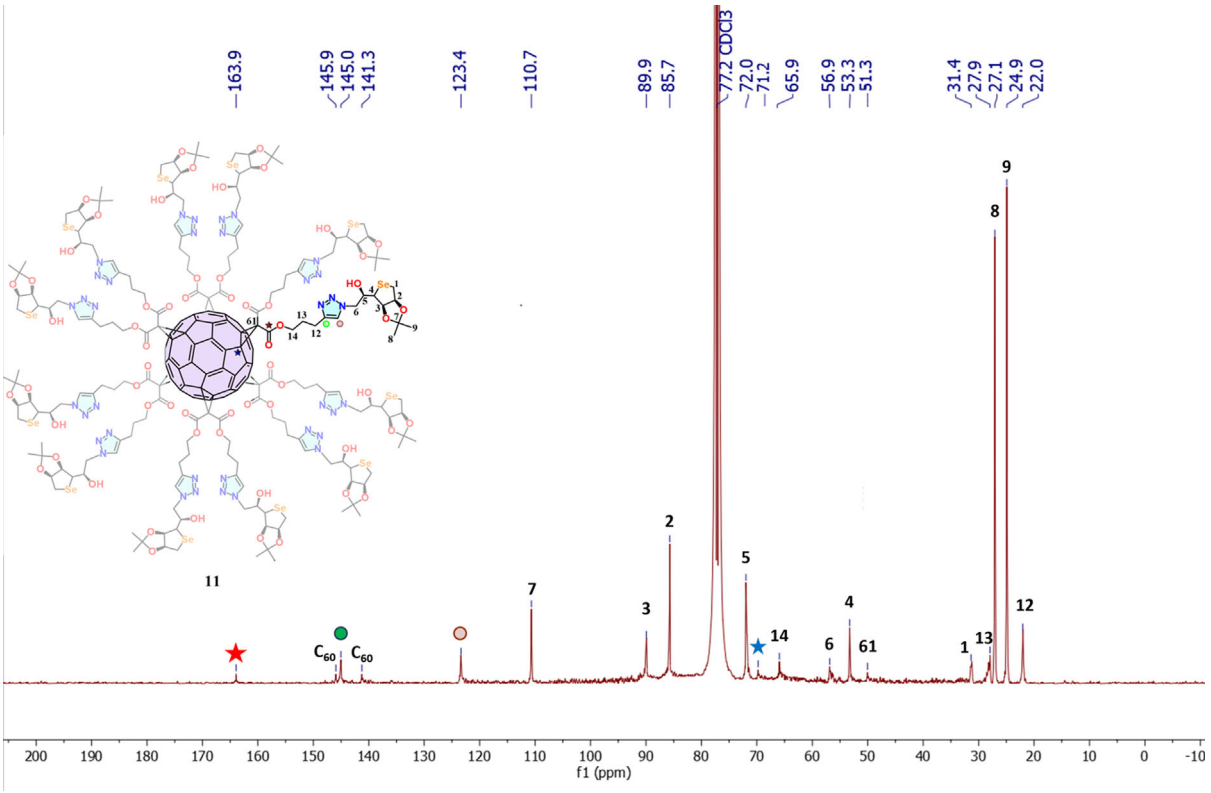

Figure 1. ^{13}C NMR spectrum of compound **11** in $CDCl_3$.

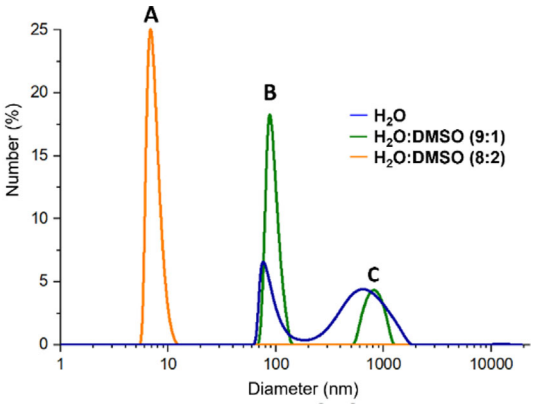

Figure 2. DLS size distribution of **11** in water solutions.

minimum energy conformation of compound **11**. Calculations capturing the noncovalent interactions (NCI) in this large-scale system predict a tendency to a relative *s-trans* conformation of the carbonyl groups of the malonate unit O═C···C═O. The results agree with those previously reported by our research group.[35] Two main interactions are reported, Se···O around 2.1 Å and OH···N 2.2 Å (nitrogen-containing five-membered rings, triazole).

The electrostatic potential map is shown in Figure 3B. From this analysis, it can be concluded that the presence of selenium, oxygen, and nitrogen atoms modifies the electrostatic potential distribution, providing three well-defined regions. In this sense, the red regions, which correlate with the oxygen atoms and the triazole rings, denote a negative density. Regions of blue color indicate positive areas somewhere in the molecule. In addition, a less significant portion of the hexakis-adduct showed neutral green regions, predicting the absence of charge separation.

The frontier molecular orbitals, highest occupied molecular orbital (HOMO), and lowest unoccupied molecular orbital (LUMO), are fundamental quantum chemical parameters to determine the reactivity of the molecules. They are used to calculate many important properties, such as chemical reactivity descriptors. In this case, the HOMO is located in the selenosugar moiety due to the presence of the selenium atom and the LUMO in the fullerene core, see Figure S21, Supporting Information. This behavior agrees with other hexakis[60]fullerene containing strong donor atoms.[36]

NCI analysis was applied to better understand the intramolecular interactions. The NCI approach is a theoretical strategy to visualize weak NCI from the topological analysis of the quantum-mechanical electron density and its reduced gradient (RDG).[37] It provides a rich illustration of strong, attractive van der Waals interactions and also steric repulsions. Different colors are provided for the interactions observed, such as green region for van der Waals interactions and red region for steric interactions. The increase of dispersion in the system favors van der Waals interaction and the NCI n $\rightarrow \pi^*$ interaction, see **Figure 4**. Three main interactions are present, one is due to the delocalization of the *p*-rich lone pair of the selenium atom of the selenosugar moiety over the π^* orbital of the triazole ring (Figure 4A). Another

Research Article
doi.org/10.1002/ejoc.202500557

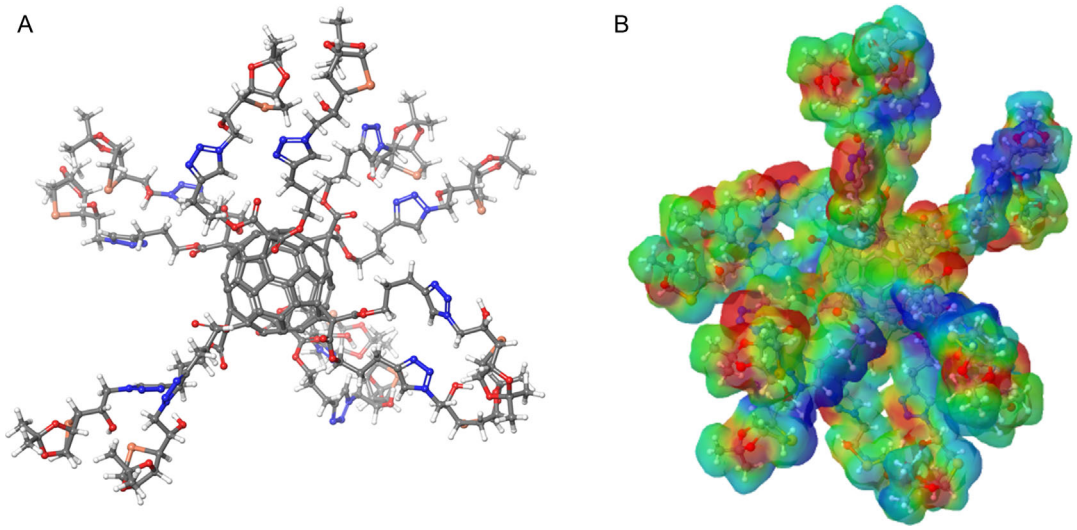

Figure 3. A) Minimum energy conformation of compound **11** obtained by the DFT-B3LYP-D3(BJ)/6–311 G(2 d,p)//PM7 level. B) Electrostatic surface potential contour. The red color represents negative potential, the blue color the positive potential, and the green color represents the uncharged regions.

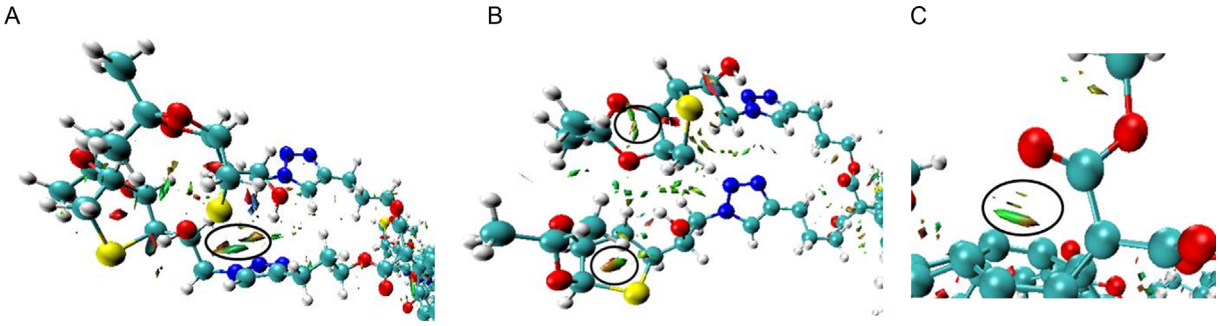

Figure 4. NCI analysis through the RGD method. Interaction type: strong attraction (blue), weak interaction (green), and strong repulsion (red).

interaction Se···H is detected by the selenium atom with the hydrogen atom with a methyl group belonging to the five-membered selenosugars (Figure 4B). Also, Figure 4C shows an interaction with the lone pair of an oxygen atom of the carbonyl group over the fullerene surface. NMR spectroscopy experiments on small model compounds and X-ray crystallographic studies confirm the presence of the $n \rightarrow \pi^*$ interaction in biomolecules and materials. It has been found that this kind of interaction plays an important role in the stability of biomolecular structures.[38]

In addition, **Table 1** shows molecular descriptors calculated for compound **11**, which are useful in studies of molecules with potential biological properties.

Topological polar surface area (TPSA) is a descriptor defined as the sum of surfaces of polar atoms in a molecule. Molecules with TPSA values greater than 140 $Å^2$ could have a low capacity for penetrating cell membranes. Drugs with higher TPSA values are less lipid-soluble and will, in general, be absorbed less extensively and more slowly. The partition coefficient (P) is a physicochemical parameter that allows determining the lipophilicity degree. It is a quantitative parameter that represents the relative solubility of a given substance in a system composed of two phases that are immiscible with each other, at a specific temperature. The logP obtained through theoretical calculations suggests that hexa-substitution with sugars induces a decrease in lipophilicity (logP = 4.25) compared to other C_{60} monoadducts containing sugars (logP ≈ 17).[15,35b] On the other hand, hydrophilicity (Hy) is a

Table 1. Theoretically calculated physicochemical parameters.

Property	Value
ΔE HOMO-LUMO–eV	2.29
Electronegativity (χ)–eV	3.59
Global hardness (η)–eV	1.15
Electrophilicity (ω)–eV	7.38
Ionization potential (I)–eV	4.74
Electron affinity (A)–eV	2.44
Softness (δ)–eV	0.87
TPSA – $Å^2$	1148.4
LogP	4.25
Hy	4.98

Research Article
doi.org/10.1002/ejoc.202500557

key factor in biodegradation in biological systems. Hy measures how well the material absorbs, swells, or dissolves in polar solvents. Chemical hardness denotes a compound's ability to resist deformation, while softness is the inverse measure. Analysis of the table reveals that the molecule is characterized as hard and more stable, indicating lower reactivity. Additionally, absolute electronegativity measures an atom's ability to attract shared electrons in a covalent bond to itself. Thus, the molecule exhibits higher electronegativity and greater charge flow.

Based on theoretical results, which suggest that **11** has low penetrability in cell membranes, and also considering that fullerene derivatives[39] and selenosugars[6a,8a] were found to possess ROS scavenging capacity, the cytotoxic effects of **11** were preliminarily assessed toward HaCaT keratinocytes, a widely used cellular model to study in vitro cytotoxicity induced by materials and chemicals.[40] Although dissolved in an H_2O:DMSO (8:2, v/v) system selected to minimize aggregation, **11** formed a thin, film-like layer upon addition to the culture medium, indicating colloidal or surface-active behavior rather than full solubility. To reflect this property, **11** was applied directly to the cell culture wells as a film-like material in the [3-(4,5-dimethyl-2-thiazolyl)-2,5-diphenyl-2 H-tetrazolium] (MTT) assay. The results revealed a concentration-dependent increase in mitochondrial redox activity, with a 25% increase in cellular metabolic activity at 100 μM compared to untreated controls (see **Figure 5**). While this may suggest a mild stimulation of cell metabolism, no definitive antioxidant or cytoprotective effect can be concluded based on the current data.

These observations were consistent with previous reports describing the cytoprotective effects of polyhydroxylated fullerenes[40] and polyvinylpyrrolidone-wrapped fullerenes[41,42] in HaCaT cells under oxidative stress. Although compound **11** shares structural features with these materials, such as a fullerene core and redox-active moieties, its biological activity remains to be fully explored. Nonetheless, its good cytocompatibility and film-forming behavior highlight its potential for further investigation in the context of material-cell interactions and biomedical applications.

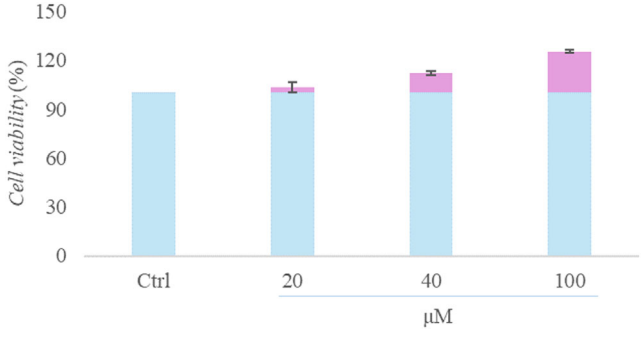

Figure 5. Cell viability (%) of **11** on the HaCaT cell line at concentration levels equal to 20, 40, and 100 μM. Ctrl = untreated control cells. Values are expressed as mean ± SD (n = 3) from three independent experiments.

3. Conclusion

Here we have reported for the first time on the synthesis of fullerene selenosugar conjugate in which the C_{60} core is surrounded by selenium-containing D-talose residues. The SeB was prepared using a multistep synthetic procedure by combining Bingel's cyclopropane methodology with the click chemistry azide-alkyne Huisgen reaction with good yield. It was necessary to use **8** to form the azide used in the final reaction step. Mass spectrometry, NMR spectroscopy (1D and 2D), UV–vis spectroscopy, and DLS analysis were used to characterize the new seleno-fullerene molecule. It is noteworthy that the high degree of symmetry (T_h) in the hexakis-adducts was revealed by NMR spectroscopy. The observed aggregation behavior of **11** suggests its potential use in biological assays in water or DMSO/H_2O. Multilevel theoretical calculations (DFT-B3LYP-D3(BJ)/6–311 G(2 d,p)//PM7) of this large-scale system predicted the minimum energy conformation indicating a tendency to a relative *s-trans* conformation of the carbonyl groups of the malonate unit O═C···C═O and that the main interactions between the appendants in the molecule are due to van der Waals and the noncovalent $n \rightarrow \pi^*$ interaction. The calculated physicochemical parameters predicted that **11** should have a low cell membrane penetrability. Furthermore, calculated physicochemical descriptors predicted low membrane permeability, prompting a preliminary cytocompatibility assessment in HaCaT keratinocytes. Under the tested conditions, **11** showed no cytotoxicity and a moderate increase in cellular metabolic activity, supporting its potential for further investigation in biologically relevant settings.

4. Experimental Section

Materials and Instrumentation

General: All reagents were of commercial quality and were used as supplied unless otherwise specified. All reactions were performed using an atmosphere of nitrogen and oven-dried glassware. Thin-layer chromatography (TLC) was performed with silica gel plates Merck 60 F254, and the display of the products on TLC was accomplished with UV lamp lighting, molecular iodine, and in H_2SO_4/MeOH (95:5) with further heating until the development of color. Column chromatography was performed using silica gel (60 Å, 32–63 μm). The NMR spectra were recorded on a Varian Inova Marker (500 MHz) spectrometer in $CDCl_3$ solution unless otherwise specified. The chemical shifts are reported in ppm (δ). The ^{1}H and ^{13}C NMR full characterization of the products was obtained based on 2D NMR. The UV spectrum was recorded in a Jasco V-750 UV–vis/NIR scanning spectrophotometer, samples were dissolved in chloroform, and absorptions λ are given in nm. FTIR spectra were recorded using the ATR mode. Samples **9** and **10** were derivatized to reduce the polarity of their free hydroxyl groups. Derivatization was carried out using 50 μL of *N,O*-bis(trimethylsilyl)acetamide (TMS) at 90 °C for 45 min. The resulting derivatives were analyzed using an Agilent 7890B gas chromatograph coupled to a 5977 A mass spectrometry detector (GC–MS). Samples were dissolved in hexane at a concentration of 50 mg L^{-1}, and 1 μL of each solution was injected for analysis. The carrier gas used in all the methods was Helium. A method involving a mass range of 30 to 600 Dalton (Da), a solvent delay of 5,50 min, was used. The initial temperature is 70 °C, for about 2 min, then reaching a temperature of 230 °C with an increase of

20 °C min^{-1}, 240 °C, and 270 °C. Fullerene derivatives **1** and **11** were resuspended in chloroform and methanol 50% 1:1 v/v. Subsequently, volumes of 0.5 μL of samples were mixed on a MALDI metal plate with an equal volume of the matrix consisting of a solution of 2 mg mL^{-1} dithranol in chloroform and methanol 50% 1:1 v/v, with 0.2% of formic acid. Mass spectrometry analysis was performed on an AB SCIEX 5800 MALDI-TOF mass spectrometer equipped with Voyager software. MS spectra were acquired in the positive mode. Mass calibration was performed using external peptide standards purchased from Applied Biosystems. The analysis of each sample involved the use of the same laser intensity and the same number of shots on the entire surface of the sample plate spot, favoring a homogeneous description of the compound of interest. Elemental analysis was performed in duplicate using a Flash Smart V CHNS instrument (Thermo Fischer).

Computational Details

Energy calculation was done at the B3LYP hybrid functional[43] together with D3(BJ)[44] correction and the 6–311 G (2 d,p) basis set,[45] taking the lowest energy conformation, a choice given the need for a balanced compromise between accuracy and computational efficiency in describing this complex molecule. Full optimization structure was carried out at the modern semiempirical method PM7.[46] PM7 was parameterized using experimental and high-level ab initio reference data. The nature of all optimized structures was determined based on the harmonic vibrational frequency calculations performed at the same level to confirm a minimum on the potential energy surface. This method combination has been extensively validated in previous studies.[47] Optimizations were done using MOPAC2016 Version: 22.234 (http://OpenMOPAC.net), and the energy calculations were done using ORCA Program Version 5.0.[48]

The reduced density gradient (RDG) analysis was performed by using the NCI theory and using the Multiwfn program (Multifunctional Wavefunction Analyzer)[49] for realizing electronic wavefunction analysis using suggested default values. For the analysis, the results were visualized with the Visual Molecular Dynamics (VMD) software.[50] Physicochemical properties were calculated by alvaMolecule software (https://www.alvascience.com).[51]

MTT Cell Viability Assay

HaCaT cells were seeded in 12-multiwell plates at a density of 1.5×10^5 cells/well. The day after seeding, cells were treated with **11** at three different concentration levels (20, 40, and 100 μM). For these treatments, compound **11** was dissolved in a H_2O:DMSO mixture (8:2, v/v). After 24 h, cells were treated with MTT [3-(4,5-dimethyl-2-thiazolyl)-2,5-diphenyl-2 H-tetrazolium] solution (0.5 mg mL^{-1}). The exposure time was set at 24 h, after which the MTT solution was removed, and the resulting formazan dye was dissolved in DMSO. Subsequently, 150 μL aliquots were transferred into a 96-well plate for absorbance measurement at 570 nm using a Victor3 Perkin Elmer absorbance reader (Perkin Elmer/Wallac, Waltham, MA, USA). Cell viability (%) was calculated relative to untreated control cells. The cell viability (%) was calculated as a percentage increase compared to untreated control cells (ctrl).

Chemical Synthesis: Synthesis of 1,4-Anhydro-2,3-O-Isopropylidene-4-Seleno-6-Tosyl-D-Talitol (9)

To a stirred solution of 1,4-anhydro-2,3-O-isopropyldene-4-seleno-D-talose (534 mg, 2.00 mmol) in anhydrous dichloromethane (28.0 mL) at 0 °C and under an inert atmosphere, tosyl chloride (460 mg, 2.40 mmol), DMAP (24 mg, 0.20 mmol), and triethylamine (574 μL, 4.00 mmol) were added. The reaction was kept at room temperature overnight. The reaction mixture was washed with ammonium chloride solution (20%) and brine. The organic phase was dried over anhydrous sodium sulfate, and the solvent was removed. The crude was purified on a silica gel chromatography column with chloroform as the mobile phase. **Yield**: 684 mg (1.54 mmol, 77%). Yellow oil. **^{1}H-NMR** (500 MHz, δ ppm): 7.78 (d, $J = 8.1$ Hz, 2 H, H11, H11′), 7.35 (d, $J = 8.2$ Hz, 2 H, H12, H12′), 4.93 (m, 1 H, H2), 4.71 (dd, $J = 5.6$, 2.2 Hz, 1 H, H3), 4.06 (m, 1 H, H_{6a}), 4.01-3.95 (m, 2 H, H5, H_{6b}), 3.57 (m, 1 H, H4), 3.23 (dd, $J = 11.3$, 5.0 Hz, 1 H, H_{1a}), 2.92 (d, $J = 11.2$ Hz, 1 H, H_{1b}), 2.45 (s, 3 H, CH_3), 1.48 (s, 3 H, H8), 1.29 (s, 3 H, H9). **^{13}C-NMR** (125 MHz, $CDCl_3$, δ ppm): 145.3 (C13), 130.1 (C12, C12′), 128.1 (C11, C11′), 110.9 (C7), 89.3 (C3), 85.3 (C2), 72.8 (C6), 71.0 (C5), 51.9 (C4), 30.2 (C1), 27.1 (C9), 24.9 (C8), 21.8 (C14). **MS** GC-MS (EI, TMS derivative): $m/z = 494.1$ $[M + TMS]^+$. **Anal**. Calcd. for $C_{16}H_{22}O_6SSe$: C, 45.61; H, 5.26; S, 7.61. Found: C, 45.65; H, 5.38; S, 7.59.

Synthesis of 1,4-Anhydro-6-Azido-2,3-O-Isopropylidene-4-Seleno-D-Talitol (10)

To a stirred solution of **9** (622 mg, 1.48 mmol) in anhydrous DMF (10.0 mL), sodium azide (380 mg, 5.92 mmol) was added under nitrogen flux. The reaction was kept at 100 °C overnight. The reaction mixture was filtered through a pad of celite and then washed with water and brine. The organic phase was dried over anhydrous sodium sulfate, and the solvent was removed. The crude was purified on a silica gel chromatography column with chloroform as the mobile phase. **Yield**: 296 mg (1 mmol, 70%). Colorless oil. **^{1}H-NMR** (500 MHz, δ ppm): 4.96 (td, $J = 5.5$, 2.6 Hz, 1 H, H2), 4.71 (dd, $J = 5.6$, 2.8 Hz, 1 H, H3), 3.82 (dt, $J = 7.1$, 4.4 Hz, 1 H, H5), 3.65 (dd, $J = 4.4$, 2.8 Hz, 1 H, H4), 3.49–3.32 (m, 2 H, H6), 3.23 (dd, $J = 11.7$, 5.4 Hz, 1 H, H_{1a}), 2.99 (dd, $J = 11.6$, 2.6 Hz, 1 H, H_{1b}), 2.43 (s, 1 H, OH), 1.52 (s, 3 H, H8), 1.31 (s, 3 H, H9). **^{13}C-NMR** (125 MHz, $CDCl_3$, δ ppm): 111.2 (C7), 89.1 (C3), 85.2 (C2), 71.9 (C5), 56.4 (C6), 53.6 (C4), 29.5 (C1), 27.3 (C9), 25.0 (C8). **MS** GC-MS (EI, TMS derivative): $m/z = 365.1$ $[M + TMS]^+$. **Anal**. Calcd. for $C_9H_{15}N_3O_3Se$: C, 36.99; H, 5.17; N, 14.38. Found: C, 37.07; H, 5.06; N, 14.50.

Synthesis of Hexakis[60]fullerene (11)

In a round flask equipped with a magnetic stirrer, **1** (32 mg, 0.017 mmol) was dissolved in DCM/H_2O (9:1, 2 mL) and **10** (52 mg, 0.17 mmol), $CuSO_4{\cdot}5H_2O$ (0.7 mg, 0.002 mmol) and sodium ascorbate (1.3 mg, 0.004 mmol) were added under nitrogen flux. The resulting mixture was vigorously stirred at room temperature for 72 h. The reaction mixture was diluted with DCM and washed with water and brine. The organic phase was dried over anhydrous sodium sulfate, and the solvent was removed. The crude was purified on a silica gel chromatography column with chloroform:methanol (95:5) as the mobile phase. **Yield**: 78 mg (0.014 mmol, 80%). Orange solid. **^{1}H-NMR** (500 MHz, δ ppm): 7.45 (m, 1 H, H10), 5.05 (bs, 1 H, H2), 4.91 (bs, 1 H, H3), 4.51-4.30 (m, 6 H, H5, H6, H14), 3.69 (bs, 1 H, H4), 3.45 (bs, 1 H, H1a), 2.97 (bs, 1 H, H1b), 2.63 (m, 2 H, H12), 2.00 (m, 2 H, H13), 1.54 (s, 3 H, H8), 1.33 (s, 3 H, H9). **^{13}C-NMR** (125 MHz, $CDCl_3$, δ ppm): 163.9 (C═O), 145.9 (Csp^2 fullerene), 145.0 (C11), 141.3 (Csp^2 fullerene), 123.4 (C10), 110.7 (C7), 89.9 (C3), 85.7 (C2), 72.0 (C5), 71.2 (Csp^3 fullerene), 65.9 (C14), 56.9 (C6), 53.3 (C4), 51.3 (C61), 31.4 (C1), 27.9 (C13), 27.1 (C8), 24.9 (C9), 22.0 (C12). **HRMS** (MALDI): $m/z = 4751.8940$ $[M–12(C_3H_6O_2)]^{\cdot+}$ Calc. for $C_{210}H_{192}N_{36}O_{36}Se_{12}$ 4752.4278.

Acknowledgements

The authors thank the financial support from the ERASMUS+ KA 171 program for international mobility financing. Y.P.-B. is

grateful for the assistance provided by Dr. Jean-Pierre Djukic´s lab (University of Strasbourg). This research was also supported by the Chilean Cluster Faraday UTEM (CONICYT-FONDEQUIP–EQM180180). Powered@NLHPC: This research was partially supported by the supercomputing infrastructure of the NLHPC (no. CCSS210001), Chile.

Open access publishing facilitated by Universita degli Studi di Napoli Federico II, as part of the Wiley - CRUI-CARE agreement.

Conflict of Interest

The authors declare no conflict of interest.

Data Availability Statement

The data that support the findings of this study are available from the corresponding author upon reasonable request.

Keywords: click reactions · cycloadditions · hexakis[60]fullerenes · organoselenium compounds · selenosugars

[1] B. C. Dickinson, C. J. Chang, *Nat. Chem. Biol.* **2011**, *7*, 504.
[2] D. Njus, P. M. Kelley, Y. J. Tu, H. B. Schlegel, *Free Radic. Biol. Med.* **2020**, *159*, 37.
[3] J. Terao, *Food Funct.* **2023**, *14*, 7799.
[4] C. Gallo-Rodriguez, J. B. Rodriguez, *ChemMedChem.* **2024**, *19*, e202400063.
[5] a) C. González, M. De Nisco, R. Lemos, G. Cimmino, Y. Pérez-Badell, S. Pacifico, S. Pedatella, *Eur J. Org. Chem.* **2025**, e202500291; b) A. Nucci, F. Marino-Merlo, M. De Nisco, S. Pedatella, F. Rossi, C. Jacob, R. Caputo, A. Mastino, *Amino Acids* **2014**, *46*, 459; c) F. Marino-Merlo, E. Papaianni, C. Frezza, S. Pedatella, M. De Nisco, B. Macchi, S. Grelli, A. Mastino, *Viruses* **2019**, *11*, 428.
[6] a) G. Cimmino, M. De Nisco, S. Piccolella, C. Gravina, S. Pedatella, S. Pacifico, *Antioxidants* **2024**, *13*, 744; b) M. J. Davies, C. H. Schiesser *New J. Chem.* **2019**, *43*, 9759; c) L. Cheng, Y. Wang, X. He, X. Wei, *Int. J. Biol. Macromol.* **2018**, *120*, 82–92.
[7] E. B. Souto, P. Severino, R. Basso, M. H. A. Santana, *Oxidative Stress And Nanotechnology*, *vol. 1028*, (Eds: D. Armstrong, D. Bharali, Humana Press, N. J. Totowa **2013**, pp. 37–46.
[8] a) G. Cimmino, M. De Nisco, C. Alonso, C. Gravina, V. Piscopo, R. Lemos, L. Coderch, S. Piccolella, S. Pacifico, S. Pedatella, *Eur. J. Med. Chem. Rep.* **2024**, *12*, 100240. b) L. Serpico, S. D. Iacono, L. De Stefano, S. De Martino, M. Battisti, P. Dardano, S. Pedatella, M. De Nisco, *Eur. Polym. J.* **2022**, *178*, 111486. c) I. Khalil, W. A. Yehye, A. E. Etxeberria, A. A. Alhadi, S. M. Dezfooli, N. B. M. Julkapli, W. J. Basirun, A. Seyfoddin, *Antioxidants* **2020**, *9*, 24.
[9] a) S. Wohlfart, S. Gelperina, J. Kreuter, *J. Control. Release* **2012**, *161*, 264. b) A. Szecskó, M. Mészáros, B. Simões, M. Cavaco, C. Chaparro, G. Porkoláb, M. A. R. B. Castanho, M. A. Deli, V. Neves, S. Veszelka *Fluids Barriers CNS* **2025**, *22*, 31–49.
[10] K. K. Cheng, P. S. Chan, S. Fan, S. M. Kwan, K. L. Yeung, Y. X. J. Wáng, A. H. L. Chow, E. X. Wu, L. Baum, *Biomaterials* **2015**, *44*, 155.
[11] R. Murugan, G. Mukesh, B. Haridevamuthu, P. S. Priya, R. Pachaiappan, B. O. Almutairi, S. Arokiyaraj, A. Guru, J. Arockiaraj, *Biomass Conv. Bioref.* **2024**, *14*, 22125.
[12] Z. Wu, L. Liu, L. Li, X. Cao, W. Jia, X. Liao, Z. Zhao, H. Qi, G. Fan, H. Lu, C. Shu, M. Zhen, C. Wang, C. Bai, *Natl. Sci. Rev.* **2023**, *10*, 309.
[13] V. Sergeeva, O. Kraevaya, E. Ershova, L. Kameneva, E. Malinovskaya, O. Dolgikh, M. Konkova, I. Voronov, A. Zhilenkov, N. Veiko, P. Troshin, S. Kutsev, S. Kostyuk, *Oxid. Med. Cell. Longev.* **2019**, *2019*, 4398695.
[14] M. Horie, A. Fukuhara, Y. Saito, Y. Yoshida, H. Sato, H. Ohi, M. Obata, Y. Mikata, S. Yano, E. Niki, *Bioorg. Med. Chem. Lett.* **2009**, *19*, 5902.
[15] R. Lemos, Y. Pérez-Badell, M. De Nisco, A. Carpentieri, M. Suárez, S. Pedatella, *ChemPlusChem.* **2025**, *90*, e202400404.
[16] R. Biswas, B. J. Manley, L. Xiao, M. J. Siringan, R. A. Crichton, J. B. Stein, A. Dawar, K. B. Lee, L. Jin, X. Li, J. Zhang, *ACS Appl. Nano Mater.* **2024**, *7*, 18036.
[17] C. Bingel, *Chem. Ber.* **1993**, *126*, 1957.
[18] A. R. Akhmetov, A. R. Tulyabaev, D. Sh. Sabirov, *FULLER. NANOTUB. CAR. N.* **2024**, *33*, 12.
[19] Z. Fejes, Á. Hadházi, E. Ruth, M. Csávás, I. Bereczki, A. Borbás, P. Herczegh, *Chem. Pap.* **2015**, *69*, 896.
[20] A. Hirsch, O. Vostrowsky, *Eur. J. Org. Chem.* **2001**, *2001*, 829.
[21] H. Li, B. Zhang, X. Li, X. Wang, F. Jia, Y. Xiao, Z. Cheng, Y. Li, D. O. Silva, H. S. Schrekker, K. Zhang, C. A. Mirkin, *Proc. Natl. Acad. Sci. USA* **2018**, *115*, 4340.
[22] I. Gallego, J. Ramos-Soriano, A. Méndez-Ardoy, J. Cabrera-González, I. Lostalé-Seijo, B. M. Illescas, J. J. Reina, N. Martín, J. Montenegro, *Angew. Chem. Int. Ed.* **2022**, *61*, e202210043.
[23] M. Palacios-Corella, J. Ramos-Soriano, M. Souto, D. Ananias, J. Calbo, E. Ortí, B. M. Illescas, M. Clemente-León, N. Martín, E. Coronado, *Chem. Sci.* **2021**, *12*, 757.
[24] S. Zhou, P. Trochimczyk, L. Sun, S. Hou, H. Li, *Curr. Org. Chem.* **2016**, *20*, 1490.
[25] I. Nierengarten, J. F. Nierengarten, *Chem. Asian J.* **2014**, *9*, 1436.
[26] J. Luczkowiak, A. Muñoz, M. Sánchez-Navarro, R. Ribeiro-Viana, A. Ginieis, B. M. Illescas, N. Martín, R. Delgado, J. Rojo, *Biomacromolecules* **2013**, *14*, 431.
[27] J. Ramos-Soriano, J. J. Reina, B. M. Illescas, N. De La Cruz, L. Rodríguez-Pérez, F. Lasala, J. Rojo, R. Delgado, N. Martín, *J. Am. Chem. Soc.* **2019**, *141*, 15403.
[28] P. Compain, C. Decroocq, J. Iehl, M. Holler, D. Hazelard, T. Mena Barragán, C. Ortiz Mellet, J. Nierengarten, *Angew. Chem.* **2010**, *122*, 5889.
[29] R. Rísquez-Cuadro, J. M. García Fernández, J. F. Nierengarten, C. Ortiz Mellet, *Chem. Eur. J.* **2013**, *19*, 16791.
[30] J. F. Nierengarten, J. Iehl, V. Oerthel, M. Holler, B. M. Illescas, A. Muñoz, N. Martín, J. Rojo, M. Sánchez-Navarro, S. Cecioni, S. Vidal, K. Buffet, M. Durka, S. P. Vincent, *Chem. Commun.* **2010**, *46*, 3860.
[31] H. Li, S. A. Haque, A. Kitaygorodskiy, M. J. Meziani, M. Torres-Castillo, Y. P. Sun, *Org. Lett.* **2006**, *8*, 5641.
[32] J. Iehl, R. Pereira de Freitas, J.-F. Nierengarten, *Tetrahedron Lett.* **2008**, *49*, 4063.
[33] M. Ruiz-Santaquiteria, B. M. Illescas, R. Abdelnabi, A. Boonen, A. Mills, O. Martí-Marí, S. Noppen, J. Neyts, D. Schols, F. Gago, A. San-Félix, M.-J. Camarasa, N. Martín, *Chem. Eur. J.* **2021**, *27*, 10700.
[34] H. Taniike, Y. Inagaki, A. Matsuda, N. Minakawa, *Tetrahedron* **2011**, *67*, 7977.
[35] a) R. Lemos, Y. Perez-Badell, O. Ortiz, L. Almagro, H. Rodríguez, M. Á. Herranz, M. Suarez, N. Martín, *Eur. J. Org. Chem.* **2024**, *27*, e202300863; b) R. Lemos, K. Makowski, L. Almagro, B. Tolón, H. Rodríguez, M. Á. Herranz, D. Molero, N. Martín, M. Suárez, *J. Org. Chem. 26*, e202201301; c) M. Suárez, K. Makowski, R. Lemos, L. Almagro, M. Ángeles Herranz, Dolores Molero, H. Rodriguez, N. F. Albericio, Y. Murata, N. Martín, *ChemPlusChem.* **2021**, *86*, 972; d) L. Almagro, R. Lemos, K. Makowski, H. Rodríguez, O. Ortiz, W. Cáceres, M. Á. Herranz, D. Molero, R. Martínez, M. Suárez, N. Martín, *Eur. J. Org. Chem.* **2020**, *2020*, 5926.
[36] F. Hörmann, W. Donaubauer, F. Hampel, A. Hirsch, *Chem. Eur. J.* **2012**, *18*, 3329.
[37] E. R. Johnson, S. Keinan, P. Mori-Sánchez, J. Contreras-García, A. J. Cohen, W. Yang, *J. Am. Chem. Soc.* **2010**, *132*, 6498.
[38] S. K. Singh, A. Das, *Phys. Chem. Chem. Phys.* **2015**, *17*, 9596.
[39] C. Pesado-Gómez, J. S. Serrano-García, A. Amaya-Flórez, G. Pesado-Gómez, A. Soto-Contreras, D. Morales-Morales, R. Colorado-Peralta, *Coord. Chem. Rev.* **2024**, *2024501*, 215550.
[40] T. Shkrigunov, Y. Kisrieva, N. Samenkova, O. Larina, V. Zgoda, A. Rusanov, D. Romashin, N. Luzgina, I. Karuzina, A. Lisitsa, N. Petushkova, *Sci. Rep.* **2022**, *12*, 21437.
[41] Y. Saitoh, A. Miyanishi, H. Mizuno, S. Kato, H. Aoshima, K. Kokubo, N. Miwa, *J. Photochem. Photobiol. B: Bio.* **2011**, *102*, 69.
[42] Y. Saitoh, H. Ohta, S. Hyodo, *J. Photochem. Photobiol. B: Bio.* **2016**, *163*, 22.
[43] A. D. Becke, *J. Chem. Phys.* **1993**, *98*, 5648.
[44] S. Grimme, S. Ehrlich, L. Goerigk, *J. Comput. Chem.* **2011**, *32*, 1456.
[45] R. Krishnan, J. S. Binkley, R. Seeger, J. A. Pople, *J. Chem. Phys.* **1980**, *72*, 650.

[46] J. J. Stewart, *J. Mol. Model.* **2013**, *19*, 1.
[47] L. Almagro, D. Hernández-Castillo, O. Ortiz, D. Alonso, A. Ruiz, J. Coro, M. A. Herranz, D. Molero, R. Martínez-Álvarez, M. Suarez, N. Martín, *Eur. J. Org. Chem.* **2018**, *2018*, 4512.
[48] a) F. Neese, . *Sci.* **2022**, *12*, e1606; b) R. Dennington, T. A. Keith, J. M. Millam, *GaussView 6.0.16*, Semichem, Inc.: Shawnee Mission, KS, USA, **2016**.
[49] F. Chen T. Lu, *J. Comput. Chem.* **2012**, *33*, 580.
[50] W. Humphrey, A. Dalke, K. Schulten, *J. Mol. Graph.* **1996**, *14*, 33.
[51] A. Mauri, M. Bertola, *Int. J. Mol. Sci.* **2022**, *23*, 12882.

Manuscript received: May 26, 2025
Revised manuscript received: July 30, 2025
Version of record online: